A validated simulation of energy harvesting with piezoelectric cantilever beams on a vehicle suspension using Bond Graph approach

Barbara Lafarge, Sébastien Grondel, Christophe Delebarre, Eric Cattan

A validated simulation of energy harvesting with piezoelectric cantilever beams on a vehicle suspension using Bond Graph approach☆

B. Lafarge*, S. Grondel, C. Delebarre, E. Cattan

Univ. Valenciennes, CNRS, Univ. Lille, Yncréa, Centrale Lille, UMR 8520 - IEMN, DOAE, Valenciennes F-59313, France

Nowadays, there is a combine effect of piezoelectric material performances and energy harvesting management strategy increase. As the same time, the energy consumption of electrical components and circuits decrease. Thus, this leads to a growing interest in recovering low energy level with piezoelectric cantilever beam in the suspensions of an automotive vehicle to perform predictive maintaining operations for example. For this pur-pose, a Bond Graph model of suspension with an embedded piezoelectric beam has been proposed since it gives the keys to find an optimal configuration for the energy harvester. The Bond Graph language is well adapted to translate multiphysics exchange of energy and power from mechanical to electrical conversion. In order to validate simulation results, a prototype of piezoelectric energy harvester has been built and tested in a laboratory environment. Furthermore, this study has been supplemented by measurements performed on a road and si-mulations are in good keeping with these proposed experimental tests. In view of an energy balance, small power but with a long duration harvesting has been obtained. Therefore, energy harvester may be interesting for a punctual use with a large period of electrical loading.

1. Introduction

With the increasing use of remote sensors embedded in vehicles, one of the primary challenges is to propose potential clean sources for powering them. At present, it is established that the piezoelectric material performances follow an intrinsic growing roadmap, and that the energy harvesting management strategy increases due to the development of new electrical power storage and restitution circuits. At the same time, the energy consumption of electrical components and circuits decreases which induces the interest for a new generation of energy harvesters.

As ambient vibrations energy are dissipated in the mechanical parts of automotive, the global aim of this work is to design piezoelectric vibrations harvesters located in a vehicle suspension. Those devices could be used for powering standalone systems, such as wireless sensors [1], or a microcontroller able to perform health monitoring of the engine by controlling the major frequencies of the rotating noise of the mechanical components of the engine [2]. Considering the wireless character of the sensors, it is not recommended to supply them with the car battery. The main advantage of using vibration energy converted by piezoelectric materials instead of batteries is to decrease the system installation price due to wiring cost for example.

In the literature, piezoelectric energy harvesters are embedded to the wheels for powering sensors and transmitting sensors data. Piezoelectric energy harvesters are bonded to the inner surface of the tire [3–7] or mounted inside [8, 9]. Others devices are also encased wholly or partially in the acoustic chamber [10], in the center face of the wheel [11] or on the rim [12].

The energy harvesting in the car could cover a wide range of natural frequencies [13–16]. In our case of study, the vibration range included from 0 to 150 Hz has a significant interest (Fig. 1) [17]. Gonçalves et al. [18] show that around 50 Hz, there are several eigenfrequencies well-known and usable.

In this paper, the authors have focused on the harvesting of the vibrations generated according to the range of frequencies between 0.5 and 150 Hz (Fig. 1-b) however due to technology limitation [19], low frequencies harvesting is difficult to realize.

Although, electro-mechanical conversion may be realized using different kinds of harvesters: electromagnetic, electrostatic, piezoelectric and so on, the authors have chosen for cost and simplicity aspects, a resonating cantilever beam made of piezoelectric material such as hard ceramic (PZT27) from Ferroperm piezoceramics.

* Corresponding author.

E-mail addresses: lafargebarbara@yahoo.fr, barbara.lafarge@univ-valenciennes.fr (B. Lafarge), sebastien.grondel@univ-valenciennes.fr (S. Grondel), christophe.delebarre@univ-valenciennes.fr (C. Delebarre), eric.cattan@univ-valenciennes.fr (E. Cattan).

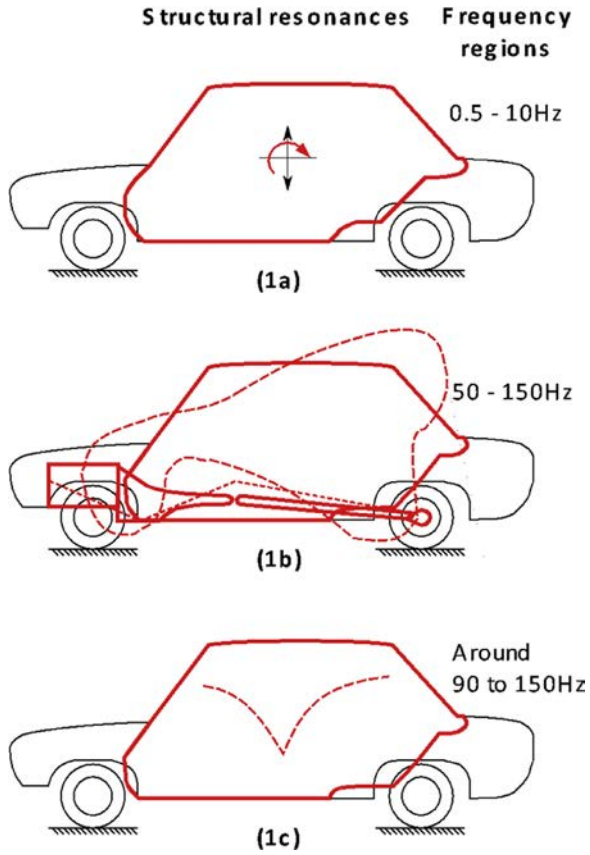

Fig. 1. The following figure shows the different and major resonances available on a car during the drive. [17] (1-a) Rigid body vibration on suspension systems and wheels, (1-b) ring mode vibration of the passenger compartment and bending vibration of driveline, and (1-c) acoustic resonance of the cavity space in the passenger compartment.

To simulate the energy harvesting cantilever system, the authors have decided to adapt and extend existing models published in the literature [20–22] and translate them in terms of Bond Graph (BG) language. Although the pure circuit method [23] or block diagrams [24] would lead to equivalent results than with the Bond Graph method for this case, the BG method was chosen due to its graphical and explicit representation of power exchanges and causality relations. Moreover, the BG method is usually more attractive and less restrictive than pure circuit models and block diagrams which consider only signal flows as indicated in reference [25]. Consequently, BG gives us an opportunity to simulate the power exchanges in the whole system. Because of its multiphysics approach it is especially suitable to optimize and forecast the whole power stored into the power storage and restitution circuit. It has already proved its use in piezoelectric energy conversion modeling [26–28] and BG model for piezoelectric beam has been developed in a recent paper [29]. Moreover, this method could also deal with nonlinear phenomena as demonstrated in reference [30]. Therefore, another advantage to use this method is that this formulation could be also easily adapted with nonlinear energy harvesters. In the literature, several overall vehicle BG models more or less complex are done with the basic structure of the suspension (wheels, suspension and chassis) and add components such as brake and steering [31] or transmission and (simplified) engine [32]. Silva et al. proposed an electric vehicle model [33] with induction motors and electromechanical interaction (ABS, regenerative brake and so on) with the possibility of variables evolution during risky situations [34]. Active suspension models are implemented with the interconnection and damping assignment-passivity based control (IDA PBC) approach [35] or quadratic form (LQR) law [36]. However, none of these BG suspension models integrated an energy harvesting cantilever system.

Moreover, the bond graph modeling approach was initially designed for the creation of lumped parameter models for a wide variety of physical and biological systems. Therefore bond graph modeling of a continuous system requires both modification and extension of the basic bond graph elements, or modification of the continuum model since without such a modification bond graph models become meaningless or useless. Hence, it is for example either possible to introduce new bond graph elements to get a continuous system [37], or to describe distribute parameters using a great number of infinitesimal lumped parameter systems such as in [38].

Furthermore, Bond graphs have proved less useful when it is desired to use control volume methods and a variable amount of matter is enclosed by the volume. To solve such a problem, a pseudo bond graph class [39] has been introduced as an extension to the bond graph method. It handles control volume problems in a natural way and retains most of the advantages of true bond graphs.

In the Section 2, this paper presents the BG modeling of a car suspension. This model is composed of several subsystems: the car suspension, the piezoelectric cantilever beam and the power storage and restitution circuits for which the equations are reminded. Then, the output power of the energy harvester subsystem is evaluated with the BG model and validated experimentally in a laboratory environment in Section 3. In Section 4, simulations of the whole system are done in order to get closer to a real study and are then compared with experimental tests performed on road.

2. Bond Graph model of the piezoelectric cantilever beam integrated on the car suspension

2.1. System description

Fig. 2-a presents the main parts of a suspension like the tire, the car damper with the sprung mass (car chassis) and the un-sprung mass (steering knuckle, tie rod, ball joint, control arm, …). For simplicity aspects, the car suspension could be represented by the quarter car system (see Fig. 2-b and -c).

It can be divided in three subsystems: the suspension, the piezoelectric cantilever beam and the storage/restitution of electrical power (see Fig. 3). In the modeling development, the piezoelectric beam is attached to the un-sprung mass.

2.2. Word Bond Graph

The Word Bond Graph (Fig. 3) is deduced from Fig. 2 and represents the global system divided into subsystems helping to have a general overview of the topic.

The input and output of each subsystem define power variables represented by a conjugated pair of force-flow variables represented by a half arrow. Power variables used for this studied system are: (force, linear velocity) = $(F, \dot{y})$ and (voltage, current) = (V,i). These BG variables are associated with mechanical and electrical harvested power respectively.

2.3. Bond Graph submodels

In this part, each word from each subsystem described in Fig. 3 is detailed and discussed.

a. Road – Suspension system

To model a vehicle suspension, the mechanical reference is the quarter car modeled by a dual-mass (Fig. 4). This model is a lumped parameters one [40]. For this reason, all the elements that compose it can be modeled as an equivalent mass, an equivalent stiffness and an equivalent damping.

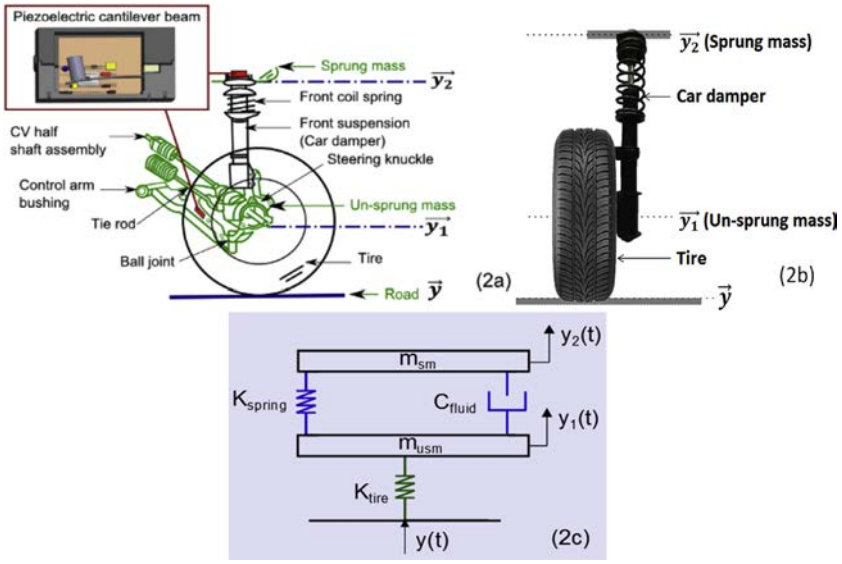

Fig. 2. Car suspension with piezoelectric cantilever beam (2-a) and quarter car system (2-b and 2-c).

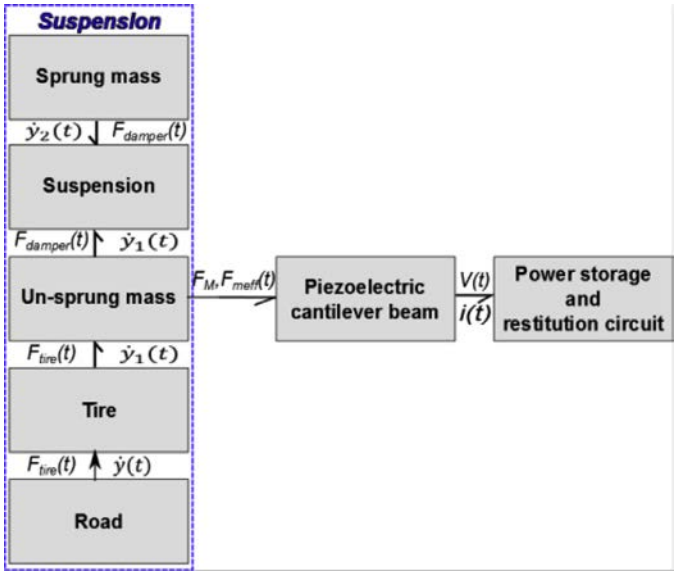

Fig. 3. Word Bond Graph of the complete system.

The parameters are deduced from the golden car suspension system [41]. The model consists of a sprung mass of m_{sm}, and an un-sprung mass of m_{usm} connected in series. The suspension is a combination of a stiffness of K_{spring} and a damper with a damping coefficient of C_{fluid}. The wheel is modeled with a stiffness coefficient $K_{tire}$for the suspension spring. The solicitation depends on the random rough road with a motion function $y(t)$ as seen in Fig. 4-a.

The governing differential equations of a dual-mass system are expressed below in (1) according to the Newton second law [42], where $y_1, y_2, \dot{y}_1, \dot{y}_2, \ddot{y}_1, \ddot{y}_2$ denote the displacement, speed and acceleration of the un-sprung mass and sprung mass respectively, and $y(t)$, $\dot{y}(t)$ correspond to the transverse motion and speed function of the road surface respectively. From (1), the frequency response and the resonances of the system could be deduced.

$$\begin{cases} m_{sm}\ddot{y}_2(t) + K_{spring}(y_2(t) - y_1(t)) + C_{fluid}(\dot{y}_2(t) - \dot{y}_1(t)) = 0 \\ m_{usm}\ddot{y}_1(t) + K_{tire}(y_1(t) - y(t)) + K_{spring}(y_1(t) - y_2(t)) + \\ C_{fluid}(\dot{y}_1(t) - \dot{y}_2(t)) = 0 \end{cases} \quad (1)$$

This couple of equation is translated in BG approach (see Fig. 4-b).

BG model of this subsystem reflects the sprung and un-sprung motions and power exchanges between mechanical elements. In this case,

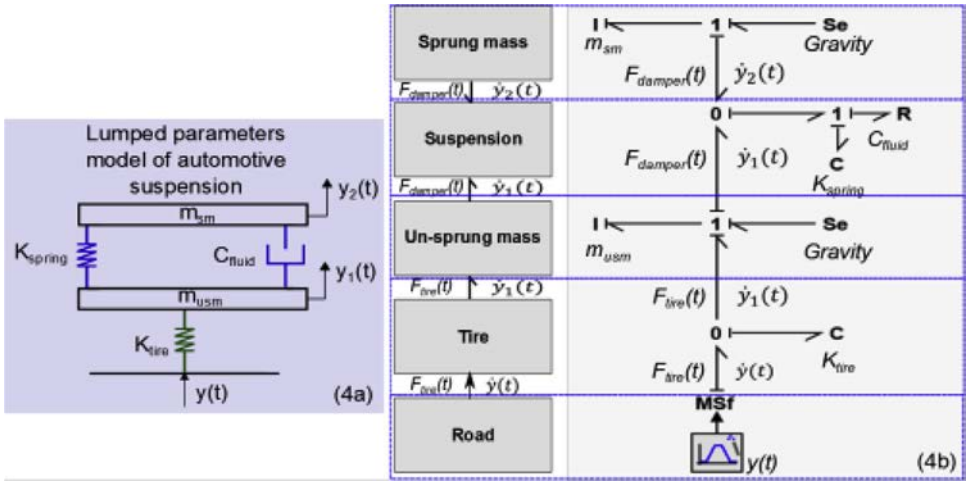

Fig. 4. Suspension representation (4-a) and road – suspension system Bond Graph model (4-b).

the BG storage elements C and I, the dissipative element R and the modulated flow source (MSf) represent the elasticity, the mass, the mechanical damping and the speed input of the road surface respectively. The 1 junction results directly from the Newton-Euler equations whereas the 0 junction reflects the velocity difference.

In the next section, the BG subsystem of the piezoelectric energy harvesting generator is presented. Several location choices of the cantilever beam are possible like the sprung mass or the un-sprung mass. In the first approach, the piezoelectric cantilever beam is placed on the un-sprung mass because the value of its acceleration is the highest as shown in Fig. 18. The information about effort and flux variables in the un-sprung mass provided by road-suspension BG are used as the inputs of this energy harvesting subsystem. Thereby, the un-sprung mass is considered like a vibration source and is at the origin of the base motion of the cantilever beam.

b. Piezoelectric cantilever beam

In order to represent the piezoelectric cantilever beam conversion, the authors have chosen to rely on the work done by Erturk et al. [20–22]. Even if the starting equations of energy conversion use a distributed approach [20], thanks to the modal superposition method, the lumped approach could be used to solve the equations. Regarding the excitation frequency range, it has been decided to operate with only the first piezoelectric cantilever beam resonance for practical purpose [22] although the BG model is also able to deal with multiple modes if necessary. Thereby, the representation of the system with lumped elements in Fig. 5 is appropriate.

Compared to PVDF polymer [43], the PZT material is easily breakable with large deformation, especially in energy harvesting application, but in return the polymer mechanical impedance compared to those of PZT is not well adapted to the mechanical structure of the suspension and the vibration coupling of the energy harvester should be too low for our application. The maximum stress endured by the piezoelectric material is around 5 MPa what represents 20% of the mean literature yield stress [44]. For this ratio, it is generally assumed that the fatigue is not leading to the rupture initiation. In addition, it has been shown experimentally that different beams could run during several hours. Therefore, the piezoelectric cantilever beam used to generate electricity is composed of two PZT27 layers with an inert center layer and an attached mass M as shown in Fig. 5. The cantilever beam is located on un-sprung mass m_{usm} (see Fig. 2). To simulate the power conversion across the piezoelectric element behavior, the cantilever beam is represented by a stiffness K_{beam} and a damper C_{beam}.

The total distributed mass M_{total} is the sum of distributed mass per length L of the beam m_{eff} and a punctual mass M applied at the end of the beam ($m_{eff} = \rho_p S_p + \rho_s S_s$, where ρ_p, ρ_s, S_p and S_s are the mass density of the PZT and the substructure and, the surface of the PZT and the substructure respectively). The electrical circuit could be represented in a first approach by a resistive load (R_{load} used in this part) and later by an electrical power storage and restitution circuit. For more detailed information, we invite the readers to refer to Erturk and co-workers [20,45].

The Eqs. (2) and (5) are the distributed parameter electromechanical equations for a cantilevered piezoelectric energy harvesting in transverse vibration.

Hence, the modal equation of motion given by the general equation [20] can be reduced to the canonical Eq. (2).

$$\ddot{\eta}_r(t) + 2\xi_r\omega_r\dot{\eta}_r(t) + \omega_r^2\eta_r(t) + \upsilon\frac{d\phi_r(x)}{dx}\Big|_{x=L} v(t) = -(m_{eff}\int_0^L \phi_r(x)dx + M\phi_r(L))\frac{d^2y_p(t)}{dt^2} \tag{2}$$

where,

$$\omega_r = \lambda_r^2\sqrt{\frac{YI_t}{m_{eff}L^2}} \tag{3}$$

and

$$\chi_r = \upsilon\frac{d\phi_r(x)}{dx}\Big|_{x=L} \tag{4}$$

The electrical equation [20] could be reduced to the modal Eq. (5).

$$\frac{C_0}{2}\dot{v}(t) + \frac{v(t)}{R_{load}} = i(t) \tag{5}$$

The effects of strain rate c_sI_t and viscous air damping c_a are substituted by the mechanical damping ratio ξ_r. ξ_r is specific to the mode and is determined experimentally.

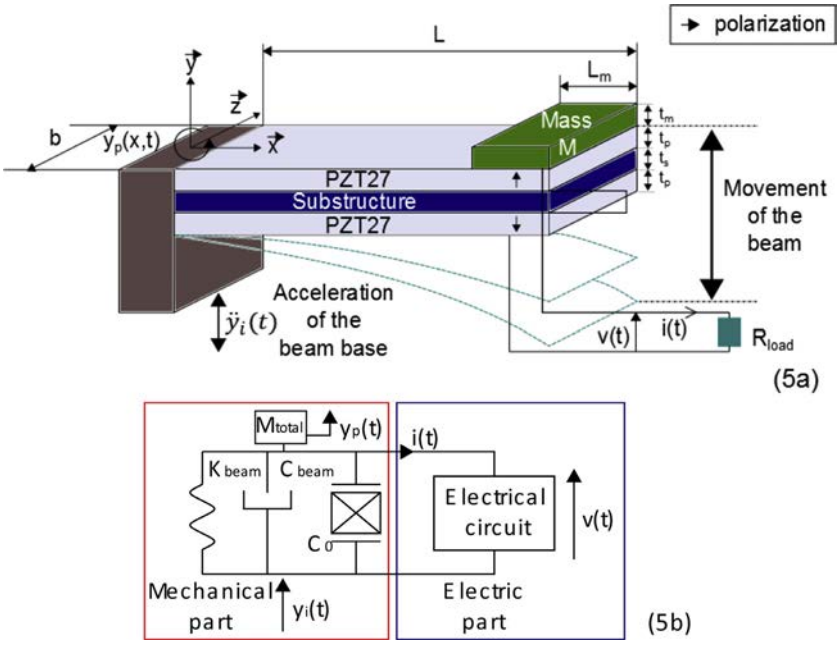

Fig. 5. A schematic diagram of the generator prototype with a load resistance (5-a) and spring-mass representation of the system (5-b).

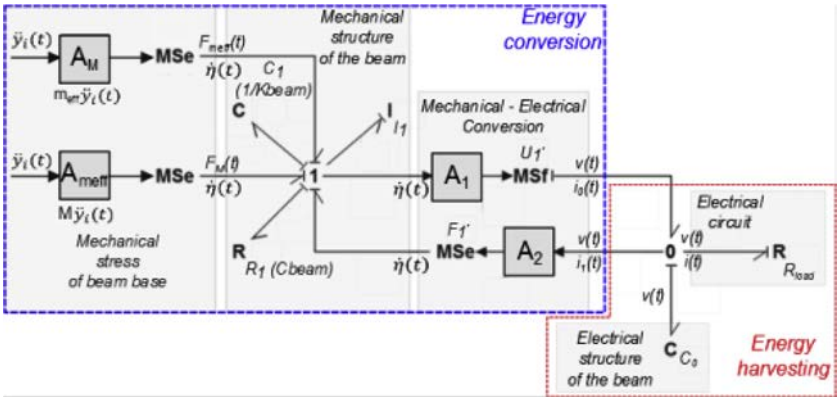

Fig. 6. Bond graph representation of the generator prototype with an external load resistance.

$$\xi_r = \frac{c_s I_t \omega_r}{2YI_t} + \frac{c_a}{2m_{eff}\omega_r} \tag{6}$$

In the following section, the authors have chosen to study only the first natural frequency of the beam ($r = 1$). Thus, the damper coefficient is written ξ_1. The output voltage across the load resistor R_{load} at the first natural frequency (7) is given by the Eqs. (2) and (5). The other resonance frequencies could be taken into account later using modal superposition to know the general behavior of the system.

$$V(t) = \frac{\frac{j\omega A_1 F_{meff}}{(\omega_1^2 - \omega^2 + 2j\xi_1\omega_1\omega)}}{\frac{1}{R_{load}} + \frac{j\omega C_0}{2} + \frac{j\omega A_1\chi_1}{\omega_1{}^2 - \omega^2 + 2j\omega\xi_1\omega_1\omega}} e^{j\omega t} \tag{7}$$

The recovered power is deduced from Eq. (7) at the resistive load, R_{load} (8).

$$P(t) = \frac{V(t)^2}{R_{load}} \tag{8}$$

Eqs. (7) and (8) are relatively easy to obtain when the piezoelectric cantilever beam system is isolated. However, their resolutions become relatively more complex when the source of the vibrations depends on another multiphysics system like the automotive suspension. Using the Eqs. (2) and (5), the BG model is deduced and shown on Fig. 6 for the first resonant mode. It should be noticed that this kind of BG model could also deal with multiple modes: for such a case, a duplication of the mechanical part is simply needed in order to represent each r mode of Eq. (2).

In the BG approach, the mechanical stress comes from the vibration sources which are divided in two efforts sources: $F_{m_{eff}}$ (9) and F_M (10) respectively. It depends on distributed (m_{eff}) and localized mass (M).

$$F_{m_{eff}} = \ddot{y}_i(t) * \left(m_{eff} \int_0^L \phi_1(x)dx \right) = A_{m_{eff}} \ddot{y}_i(t) \tag{9}$$

$$F_M = M\phi_1(L)\ddot{y}_i(t) = A_M \ddot{y}_i(t) \tag{10}$$

The mechanical behavior of the cantilever is illustrated by a normalized spring-mass system (I_1 (11), R_1 (12) and C_1 (13)). I_1, R_1 and C_1represent kinetic energy, dissipative energy and potential energy respectively.

$$I_1 = 1 \tag{11}$$

$$R_1 = c_{beam} = 2\xi_1\omega_1 \tag{12}$$

$$C_1 = \frac{1}{K_{beam}} = \frac{1}{\omega_1^2} \tag{13}$$

Generally, the electromechanical coupling is modeled as a transformer with a turn ratio [46]. But in our case of study, the electrical modal coupling term obtained with the electrical circuit Eq. (5) and the mechanical modal coupling term (4) from the differential equation of motion given by Eq. (2) are different and are represented with the mechanical-electrical coefficients A_1 (14) and A_2 (15) respectively. For this reason, the mechanical-electrical conversion that depends on the configuration, are represented by modulated sources (ensuring the exchanges of energy). The mechanical-electrical conversion is made with effort (*MSe*) and flux (*MSf*) sources according to the expression (9) and (10) respectively.

$$A_1 = e_{31}\frac{b(t_s + t_p)}{2}\frac{d\phi_1(x)}{dx}\bigg|_{x=L} \tag{14}$$

$$A_2 = e_{31}\frac{b\left(\frac{t_s}{4}{}^2 - \left(t_p + \frac{t_s}{2}\right)^2\right)}{2t_p}\frac{d\phi_1(x)}{dx}\bigg|_{x=L} \tag{15}$$

where e_{31} is a piezoelectric constant, t_s and t_p are the thickness of the substructure and the PZT respectively. The internal capacity C_0 of the piezoelectric element is modeled with a C element (16).

$$C_0 = \varepsilon_{33}^S \frac{bL}{2t_p} \tag{16}$$

where ε_{33}^S is the permittivitypiezoelectric.

The 0 junction reflects the same voltage results and gives us directly the voltage recovered of the energy harvester output across the electrical circuit, reduced here to the resistive load with element R. The value of R_{load} depends on the application and the expected results.

In reality, the power management is done according to a complex electrical circuit with a variable resistive load.

c. Power storage and restitution

In order to store power and to restitute harvested energy by piezoelectric generator, one may use a commercial component proposed by manufacturers [47]. For this reason, an electronic circuit was integrated into our BG model (Fig. 7).

The main components of this subsystem are the diode bridge (rectifying the output voltage), the buck converter (DC-to-DC power convert), the storage element (condensator) and the power management. The V_{PGOOD} signal gives an indication if the output voltage is well regulated, available and sufficient (Fig. 7). V_{PGOOD} is powered during

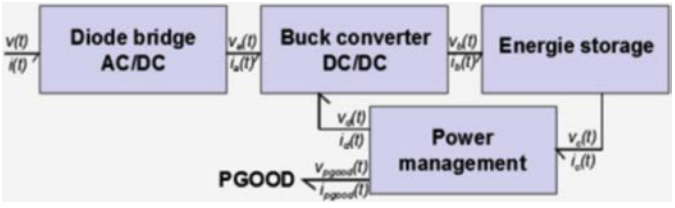

Fig. 7. Word Bond Graph of power and storage subsystems.

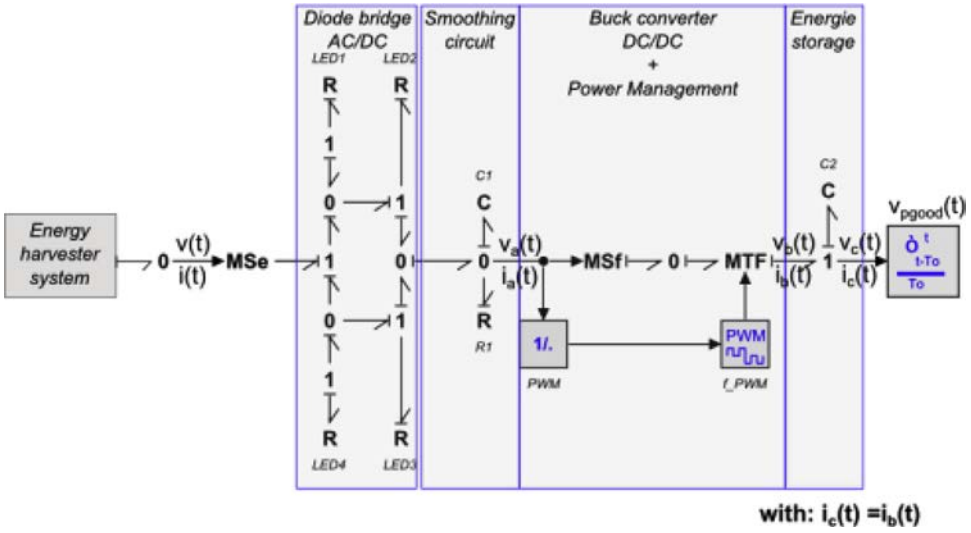

Fig. 8. Bond Graph representation of power storage and restitution circuit.

this period. The microcontroller enters into sleep state in which both input and output currents are minimal (power unsufficient). The buck converter turns on and off as needed to maintain regulation. An algorithm may be implemented in order to turn on the circuit only when the user needs to do a test over a short period, for example to control structural health monitoring.

This BG model (Fig. 8) is able to estimate the output voltage $V_{pgood}(t)$ according to the output voltage $V(t)$ of the energy harvester system. The diode bridge is illustrated by four specifics R elements (R_{LED1}, R_{LED2}, R_{LED3} and R_{LED4}) adapted to simulate the diode behavior. The smoothing circuit is done with dissipative C_1 and potential R_1 elements. The buck converter function is realized with the combination of the *MTF* element and a PWM signal. The final harvested energy is stored in C_2 element as a super capacity.

d. Global system modeling

Fig. 9 shows us the global BG model of the recovering energy mechanical vibration of the un-sprung mass. The interconnections appear clearly between all subsystems represented in the word Bond Graph. For this full model, key measurements needed are: linear velocity of the tire $\dot{y}$ and the un-sprung mass acceleration of the vehicle and the output voltage of energy harvesting system v. The acceleration gives us the forces $F_{m_{eff}}$ (Eq. 9) and F_M (Eq. 10) of the convertor base, to inject in the energy conversion subsystem whereas $\dot{y}_p$ gives us the deflection speed of the beam.

This model is able to estimate the power recovering of the cantilever according to any surface modification of the road.To this end, the real road profiles according to the IRI (International Roughness Index) [48] standard must be injected across the variable y.

3. Energy harvesting validation in laboratory environment

In order to simulate the global system, the energy harvesting subsystem model needs first to be validated on a simple case. The experimental protocol is similar to the design assumptions of the BG global model, see on previous parts. The first tests are done on a simple beam prototype without a mass on the tip and a simple external load resistor. Subsequently, the experimental and simulated results are compared. The second tests are done with a mass and the results are also compared to simulation results.

3.1. Experimental setup

By using the proposed BG model, the harvester shown in Fig. 5 is studied. The simulation is done on 20Sim software. is the based

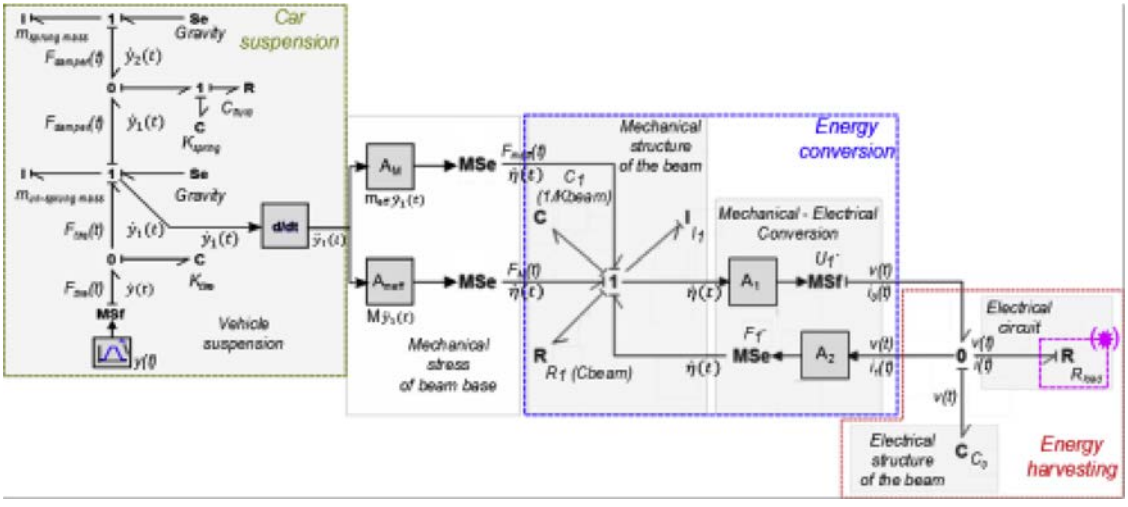

Fig. 9. Example of global system modeling with the convertor integrated to the un-sprung mass.

Table 1
Geometric, material, and electromechanical parameters of the energy harvester system.

Parameters		Values	Unity
ρ_p	Mass density of the PZT27	7700	Kg/m^3
ρ_s	Mass density of the substructure	2698.9	Kg/m^3
L	Length of the beam	65	mm
b	Width of the beam	13	mm
t_p	Thickness of the PZT27	0.58	mm
t_s	Thickness of the substructure	0.2	mm
Y_p	Young's modulus of the PZT27	76.9	GPa
Y_s	Young's modulus of the substructure	70	GPa
d_{31}	Piezoelectric constante	−170	pm/V
ε_{33}^s	Permittivity	3500	nF/m
R_{load}	External resistive load	–	Ω
M	Mass attached to end of the beam	0	kg

acceleration of the cantilever and is considered like the only input variable of the subsystem from the basic presumption. This acceleration is imposed to the two effort sources F_M and F_{meff}. All the other parameters are dependent on the configuration choice [Table 1] or are identified experimentally like the value of the damping ratio ξ_1 of the global beam. As the damping ratio is given by the logarithmic decrement of free vibrations, it can be easily deduced by measuring the free structures displacements induced by an applied force on the structure.

Then the final values v and i are observed at the end of the simulation process. For the global power harvested at the output of the converter dissipated on an optimal load, the voltage and power frequency response are observed (for example in Figs. 13–15). To link simulation and experience, the input acceleration is imposed through a shaker (Tira S50018) to the beam as shown in Fig. 10 and then the generated power is observed and compared to the simulation data. For this purpose, a generator prototype was made from two layers of PZT27 with an inert center layer (Fig. 5).

3.2. Validation of the model on a single beam with external resistor

To validate the piezoelectric cantilever BG submodel, the frequency voltage and power output are studied for the case of a resistive load R_{load} and an excitation by the shaker (Fig. 10). Moreover the frequency range of interest vary from 0 to 200 Hz [22] and the divergence between BG multimode model and BG single mode model has been evaluated for this case in Fig. 11: obtained frequency divergence is 0.0212% on the first mode whereas its amplitude increases slightly with the number r of modes: 0%, 0.3%, 0.45% and 0.6% when $r = 1,\ 2,\ 3$ and 4 respectively with a resistance value of 100 kΩ. As a result, only the first mode will be studied in the following.

The generator prototype was tested by exciting it with vibrations of 1m^2/s. To obtain these results, the simulated value of the first frequency damping ratio is equal to $\xi_1 = 0.039$, whereas the internal piezoelectric capacitance is $C_0 = 0.225$nF and the mass at the end of the beam is zero ($M = 0$).

The voltage and power outputs are given by the Eqs. 7 and 8 plotted

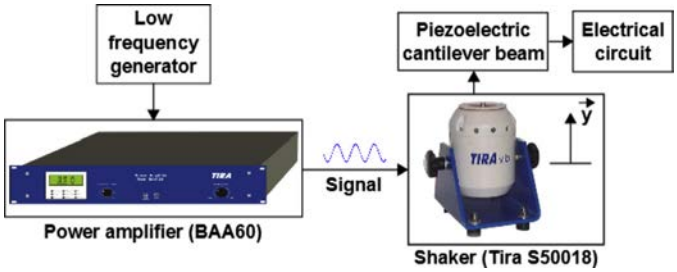

Fig. 10. Tests equipment: power generator, shaker with piezoelectric cantilever beam and scope.

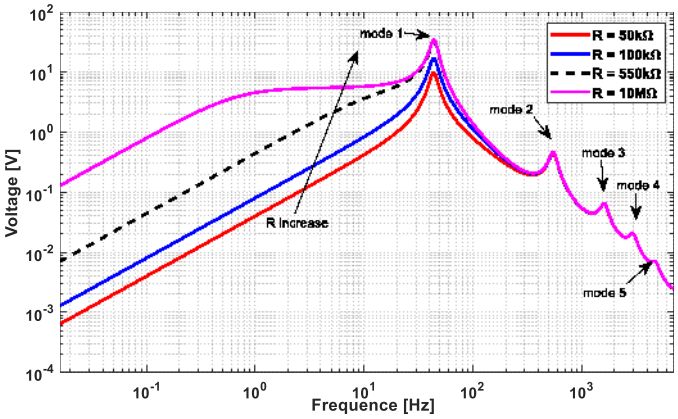

Fig. 11. Simulated voltages for value of load resistance of 50 kΩ, 100 kΩ, 550 kΩ and 10 MΩ respectively.

in Figs. 13–15 respectively. As expected, it can be noticed that the value of the load resistance R_{load} has an important impact on the dynamic behavior of the system i.e. on both the amplitudes of the voltage and the power around the resonance frequency. Figs. 13–15 show that the amplitude of the voltage increases with increasing load resistance for all ranges of frequencies.

However, the amplitude of the power is maximum for an excitation at the first resonance with a certain value of load resistance (Fig. 12). In other words, the maximum power is obtained for $f = 91$Hz with the optimal impedance. It requires that the impedance of the piezoelectric beam matches to the output impedance of the external load to maximize the power transfer. In our configuration, the impedance matching is obtained when the resistance value is around $R_{load} = 122$kΩ. This resistance value is considered optimal for the first vibration mode. This first resonant $f = 91$Hz of the beam is high but as the PZT material is easily breakable with large deformation, the low-frequency resonant is difficult to reach. To reduce the frequency resonant, a tip mass is added to the piezoelectric beam in the next subsection.

For $R_{load} = 22$kΩ (Fig. 13) and $R_{load} = 222$kΩ (Fig. 15), as expected these power amplitudes are lower. The power amplitude is equal to 1 mW and 1.4 mW respectively. The maximum voltage and power amplitude are around 13 V and 1.4 mW for the optimal load resistor respectively.

Only one mode (first resonance frequency) is obtained experimentally and is visible on the three curves with difference values of load resistance. The presence of this unique mode validates the use of the lumped parameters in the beam BG model. As expected, the experimental and simulation results are totally consistent and validate our piezoelectric cantilever beam without mass M.

3.3. Validation of the model on a beam with external resistor and mass at the tip of the beam

To ensure that the beam resonance matches the vehicle vibration mode, a mass equal to 10 g at the tip of the cantilever is empirically added. Thereby, the power generation is enhanced because the mechanical stress is higher in this case than for the natural vibration mode. Hence, the frequency range is respected. Likewise, the frequency could be yet reduced to obtain a maximal amplitude power by adjusting the geometry of the beam.

The prototype is mounted into a shaker (Fig. 16). For this new experiment, the estimated beam damping ratio was $\xi_1 = 0.08$. The acceleration of the shaker is 0.6m^2/s with the same range of frequencies as seen above (Section 3.2). To understand and to control the dynamic behavior of the beam, the voltage and power curves are plotted in Fig. 17 as function of frequencies, with the same optimal load resistance ($R_{load} = 122$kΩ) but with an attached mass M ($M = 10$g). The matching

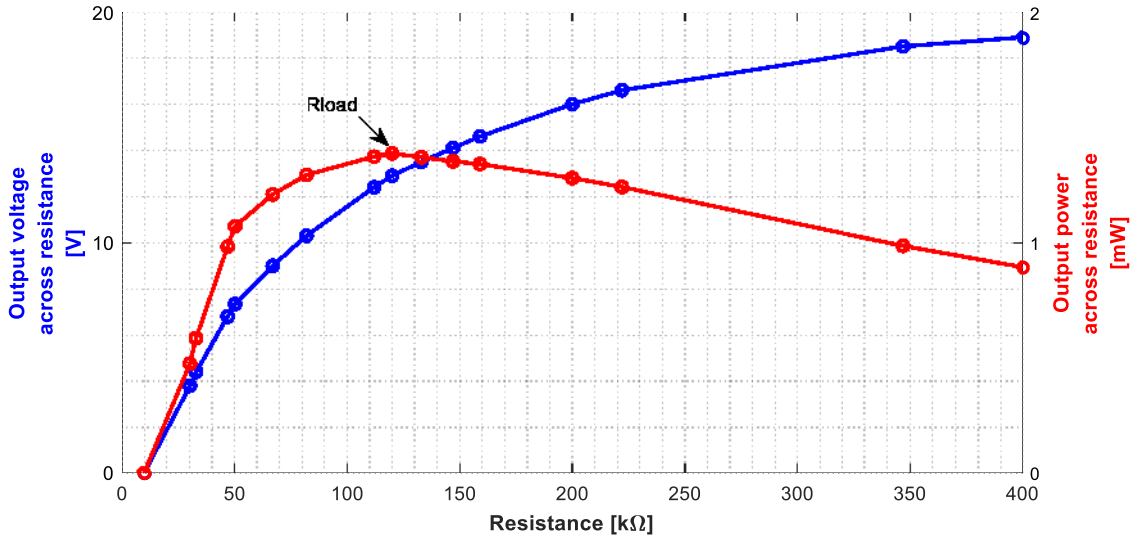

Fig. 12. Measured powers and voltages for several values of external load (first vibration mode, $f_0 = 91$Hz).

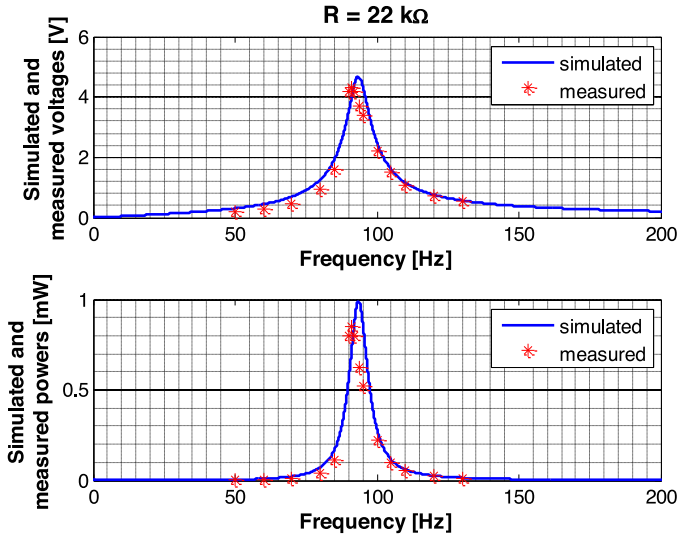

Fig. 13. Simulated and measured powers and voltages for value of load resistance of 22 kΩ.

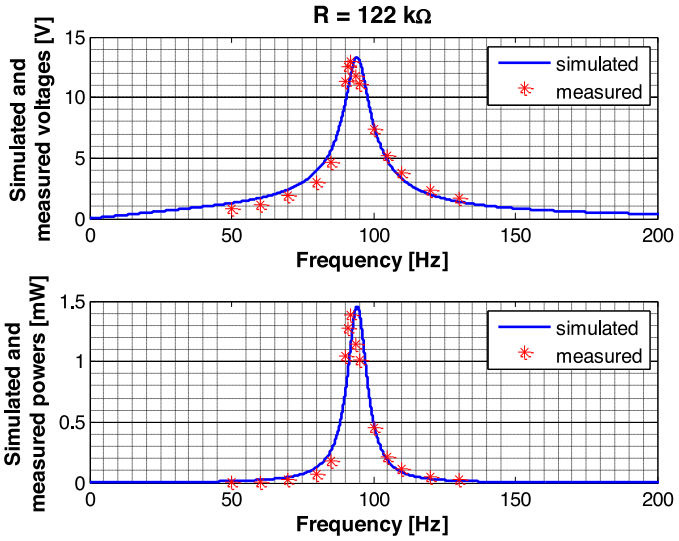

Fig. 14. Simulated and measured powers and voltages for value of load resistance of 122 kΩ.

impedance is still 122 kΩ because the tip mass does not have a high impact on the impedance of the piezoelectric structure of the beam. The first natural frequency is close to 43.5 Hz as well as one of the vehicle's eigenfrequencies. It is within the expected range. Again, the gap between measurement and simulation data is less than 10%. The obtained maximum voltage and power amplitude are around 12 V and 1.1 mW respectively.

In the next section, this new beam BG configuration is integrated into the global BG model, in order to simulate the behavior of the harvester embedded in a car suspension (Fig. 2) in view of an energy balance in the car suspension.

4. Energy harvesting with the whole system: simulation and measurements

The global simulation is now developed using simultaneously the piezoelectric cantilever beam submodel, the suspension car submodel and the electrical circuit submodel (Fig. 9). The values of the parameters (Eq. 1) for the car suspension correspond to those of a *Renault Laguna GT* [49]. In order to estimate the output power of harvested by the piezoelectric cantilever beam, the electrical circuit is reduced first to an external load. Second, a power storage and restitution circuit is placed at the output of the energy harvester since this circuit gives results that are more consistent with reality. The input mechanical stresses of the whole BG model are adapted in order to get closer to a real case of study as the passage of a car on a speed bump at 30 km/h (Fig. 18). The mechanical input solicitation is a standard speed bump. Finally, simulations performed on road with the whole BG model are then compared with experimental tests.

4.1. Simulation of the global model on a single beam with external resistor

The piezoelectric cantilever beam is mounted into un-sprung and the sprung masses of the car suspension with at the end an external load. In the same way as in the previous section, the optimal load resistance is $R_{load} = 122$kΩ and the empirical chosen mass M is 10g.

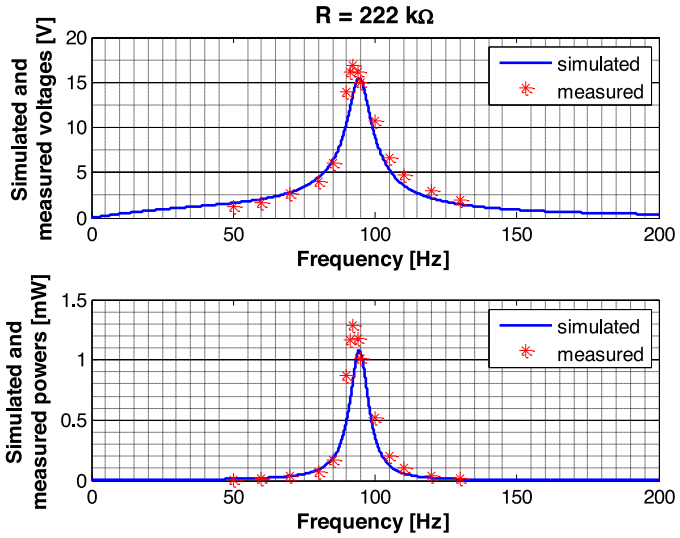

Fig. 15. Simulated and measured powers and voltages for value of load resistance of 222 kΩ.

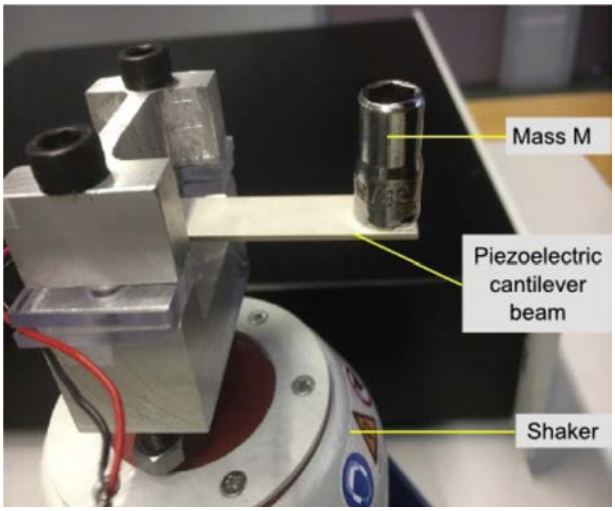

Fig. 16. A generator prototype made from PZT27 mounted into a shaker used for testing with a mass *M*.

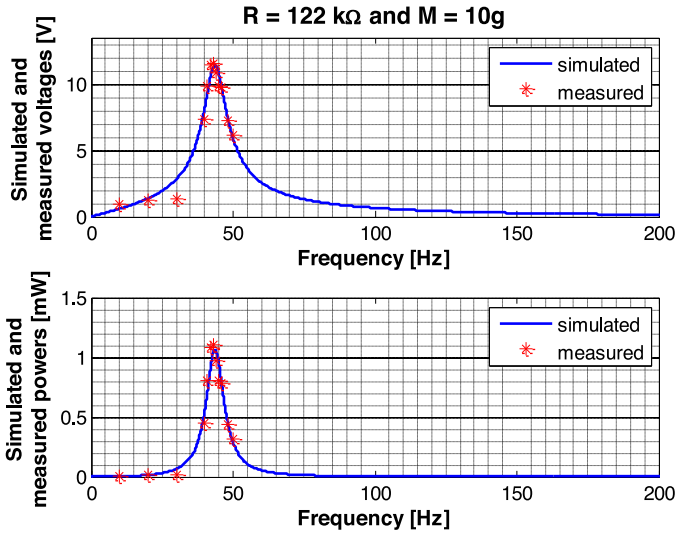

Fig. 17. Simulated and measured powers and voltages for value of load resistance of 122 kΩ and mass ($M = 10$ g).

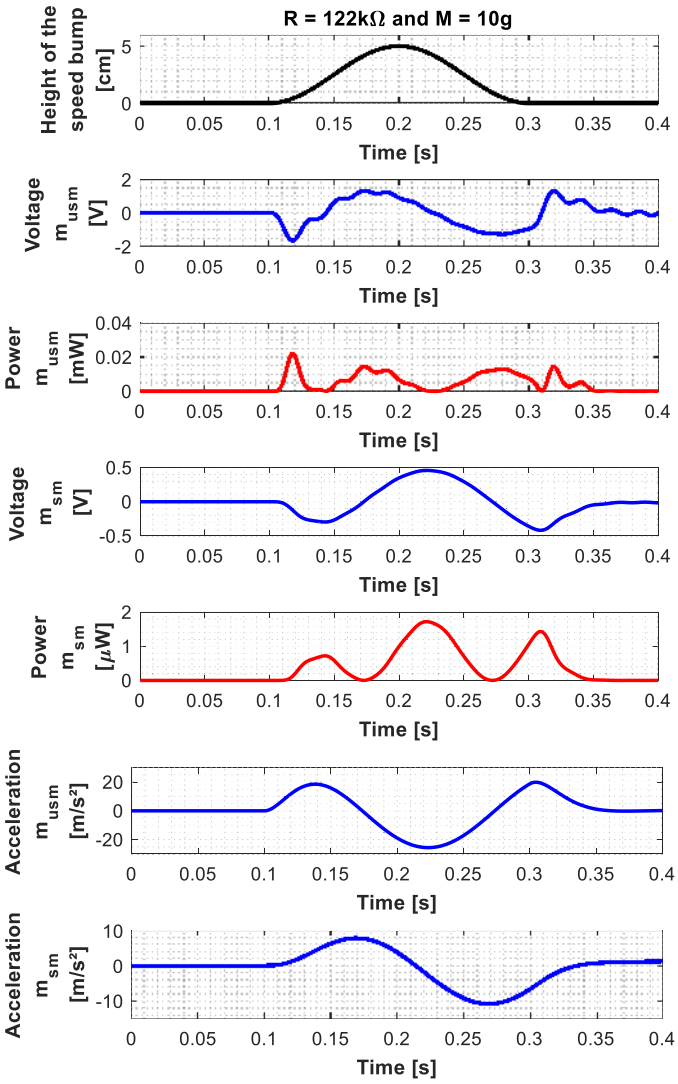

Fig. 18. Simulated voltages and powers with an optimal external load in our case of study.

Results are presented in the Fig. 18. As expected, the harvested energy is higher when the harvester is attached to the un-sprung mass. In fact, the amplitude of the movement of the un-sprung mass is greater than on the sprung mass.The maximal output voltage range obtained is close to 2 V with a maximal output power of 0.02 W during the speed bump solicitation when the mass is attached to the un-sprung mass.

4.2. Simulation of the global model on a single beam with the power storage and restitution circuit

In the next section, a power storage and restitution circuit (Fig. 7) is placed at the tip of the piezoelectric cantilever.

The Fig. 19 represents the input voltage of the storage circuit ($V(t)$), the rectified and smoothed voltage ($V_a(t)$) and the output voltage of the energy harvester ($V_{pgood}(t)$). The maximal input voltage is around 12 V whereas the maximum rectified and smoothed voltage is close to 8 V. It can be noticed that the output power of this circuit is sufficient to supply a LED or any other circuit with low consumption ($P_{max} = 0.33$W for DC voltage) during 0.3 s (Fig. 19).

To know energy distribution in the global system, it is relevant to study its evolution in all the subsystems (Figs. 20 and 21). The injected

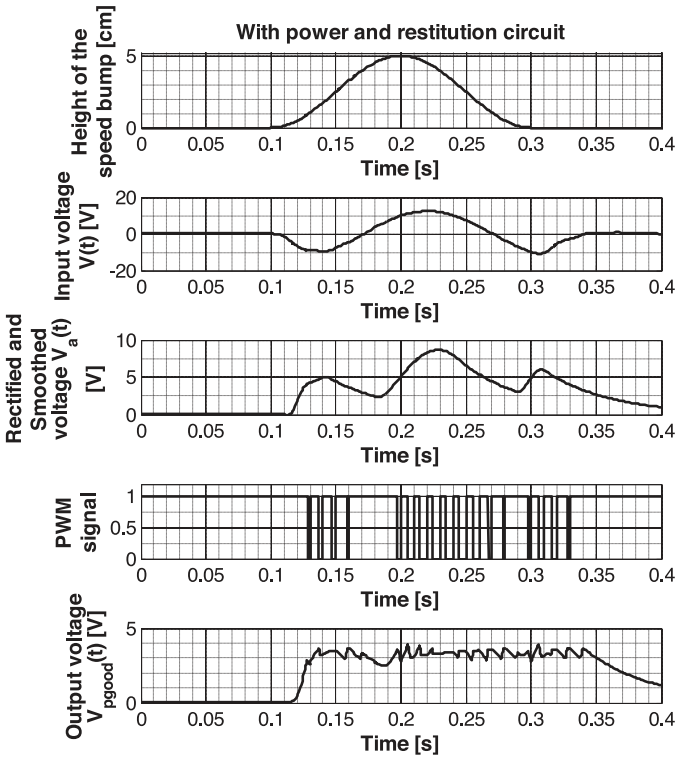

Fig. 19. Simulated voltages with power storage and restitution circuit in our case of study.

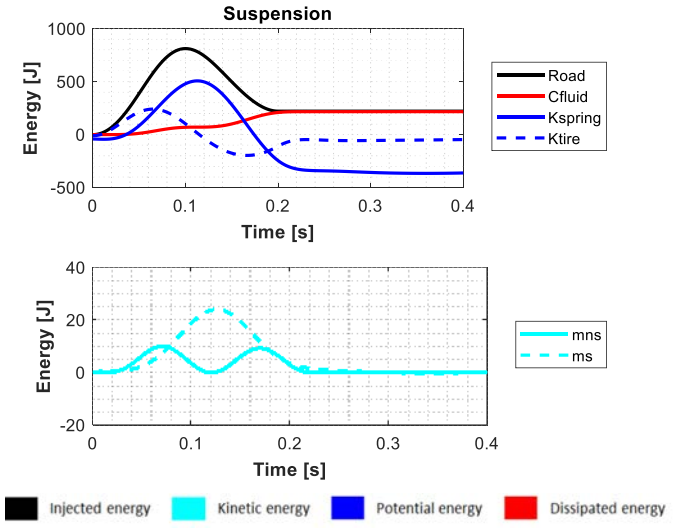

Fig. 20. Evolution of total injected energy (in black), total kinetic energy (in cyan), total potential energy (in blue) and total dissipated energy (in red) for the suspension subsystemin our case of study. (For interpretation of the references to colour in this figure legend, the reader is referred to the web version of this article.)

energy to the suspension parts by the road is 812 J computed by the model. This energy is decomposed in three different energies. The main part is dissipated through friction in the car damper (C_{fluid}) and in the cantilever beam (C_{beam} and R_{load}). In parallel, less quantity is stored in potential energy (K_{tire}, K_{spring} and K_{beam}) and in kinetic energy ($M_{un-sprung}$, M_{sprung} and I_1). Fig. 20 illustrated the total energy, i.e. the injected, dissipated and stored (potential and kinetic) energy as

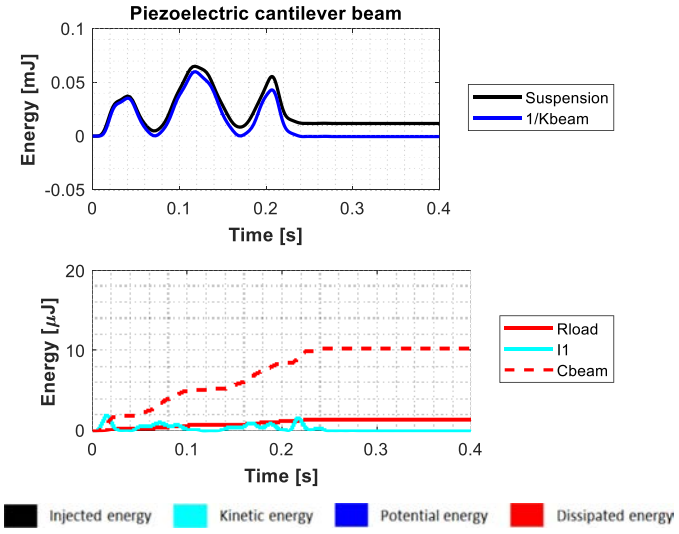

Fig. 21. Evolution of total injected energy (in black), total kinetic energy (in cyan), total potential energy (in blue) and total dissipated energy (in red) for the piezoelectric cantilever beam subsystem in our case of study. (For interpretation of the references to colour in this figure legend, the reader is referred to the web version of this article.)

function of the time, in the mechanical parts of the suspension. The obtained responses reflect the behavior of a dual-mass for the mechanical domain. Between 0 s and 0.1 s, the car goes up to the speed bump and goes down from 0.1 s to 0.2 s. After 0.2 s, there is no variation of the road height. Indeed Fig. 20 shows that the K_{tire} stored energy increases first between 0 s and 0.1167 s which means that the injected energy is stored in the first mechanical part closest to the road, then the K_{spring} stored energy in second time between 0.036 s and 0.17 s. The energy begins to dissipate in C_{fluid} at 0 s. As the injected energy is stopped to increase at 0.26 s and that all this energy is transferred to all mechanical elements, the stored and dissipated energy tend towards zero. Finally when the injected energy is constant, the system comes to the stable state. The kinetic energy ($M_{un-sprung}$ and M_{sprung}) are lower compared to the other energies.

It was also possible to determine the injected, dissipated and stored energy in the piezoelectric cantilever beam for mechanical and electrical domain (see Fig. 21). The injected energy to the beam by the suspension is 0.065 mJ computed by the model. The obtained responses reflect the behavior to a spring-mass-damper system for the mechanical domain and to electrical circuit (R_{load}) for the electrical domain. Fig. 20 shows that the mechanical energy behaves the same way. The dissipative mechanical energy in R_{load} is really low and is 1.42 μJ computed by the model. From these curves, it was also possible to determine the piezoelectric energy efficiency $\eta_{piezo} = 8.\ 10^{-8}$.

Although the power required to directly power a system to perform predictive maintaining operation, for example, is not reached with our technology, this system should work intermittently by carrying out regular checks. The reasoning is not done in terms of power but in terms of accumulated energy and necessary charging time. Energy and power are linked by this equation: $E = P_1\Delta t_1 = P_2\Delta t_2$, with $P_1 = 0.01$W (the recovered power), $P_2 = 0.33$W (the consumption of the circuit to be supplied) and $t_1 = 2$s (the control time). The time interval t_2 between two operations is deduced, $t_2 = 66$s. Also, the time ratio is $t_2/t_1 = 33$. Thus the system which it is proposed to obtain is a unique system recovering energy and carrying out the operation of structural health monitoring.

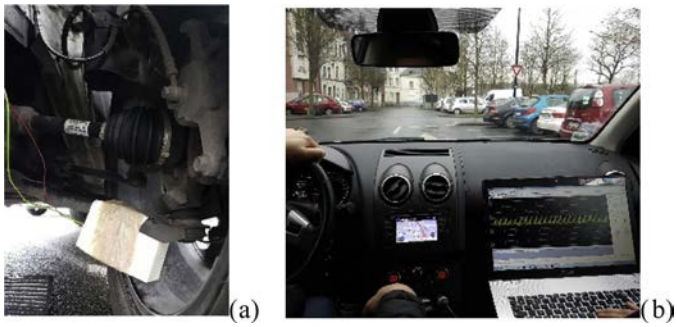

Fig. 22. Cantilever energy harvester embedded on the un-sprung mass of the small size vehicle (a). At several drive speeds, drive tests are conducted (b).

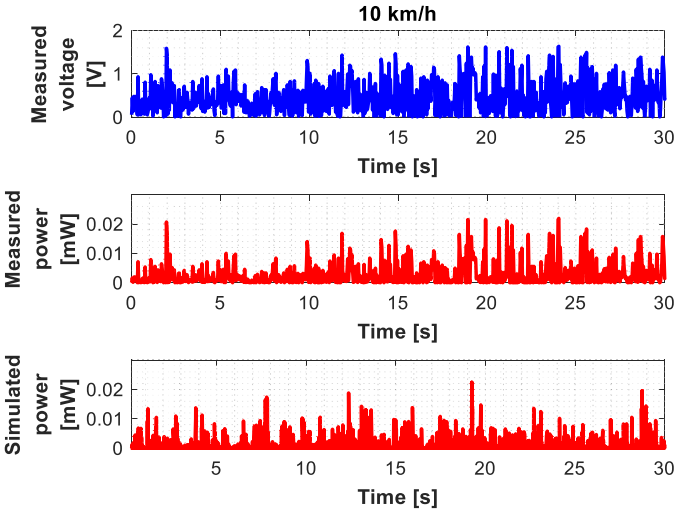

Fig. 23. Comparison between experiments and simulations in case of artificial profiles with a car speed of 10 km/h.

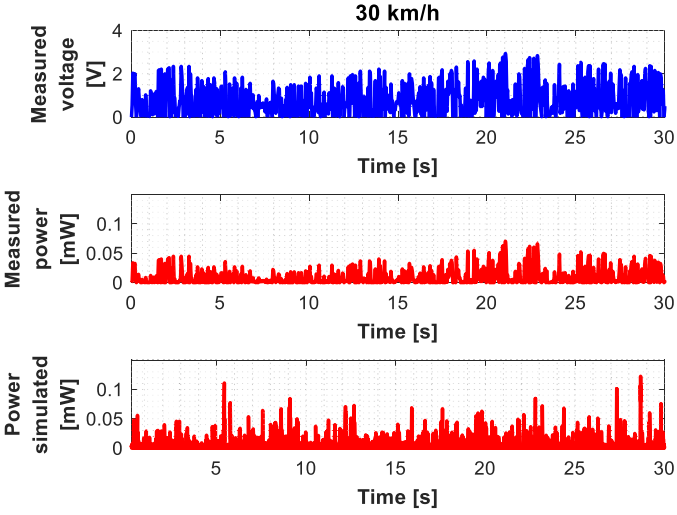

Fig. 24. Comparison between experiments and simulations in case of artificial profiles with a car speed of 30 km/h.

4.3. Experimental investigation in a real case

In order to demonstrate the validity of the approach in a real case, experimental tests have been performed with the whole energy harvester system embedded in a car (Fig. 22). Moreover, two different

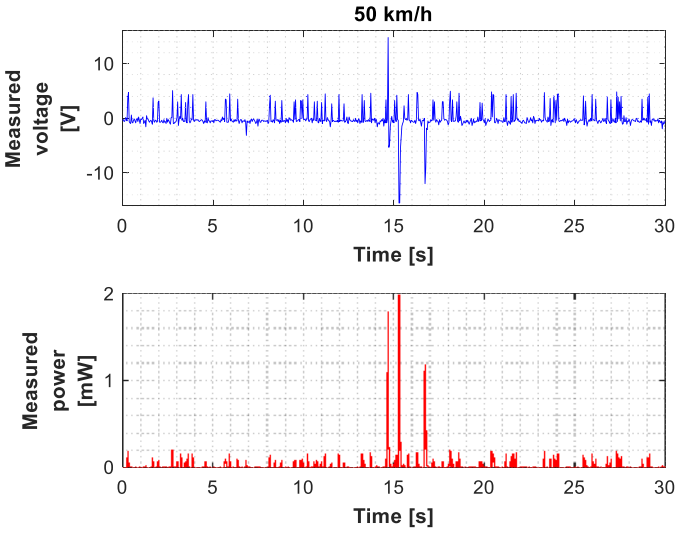

Fig. 25. Measured voltages and powers in case of driving through tramway crossing with a car speed of 50 km/h.

situations have been experimented: the first situation corresponds to drive tests on a road at 10 km/h (Fig. 23) and 30 km/h (Fig. 24) respectively, whereas the second situation coincides with the driving through a tramway crossing (Fig. 25).

From the Figs. 23 and 24, it can be noticed that the power is low whatever the speed of the vehicle. The value is in the order of 0.001 mW to 0.021 mW at 10 km/h (Fig. 23) and varies between 0.01 mW and 0.07 mW at 30 km/h (Fig. 24). However, the energy on a long period is significant and could be used to supply sensors.

Simulations with the whole BG model have also been performed on the same situation. The analysis of the simulated harvested power signals with a generated artificial profile [50] based on the equation provided by ISO 8608 standard at 10 km/h (Fig. 23) and at 30 km/h (Fig. 24) demonstrates a good keeping with the experimental results since the range of values is of the same order.

Fig. 25 gives the measured values when the car crosses tramway rails with a 50 km/h speed. One can clearly see the large vibration occurring at $t = 15$s providing a harvested power peak of 1.97 mW. In the future work, the whole system with the road profile of a tramway can also be modeled and be simulated.

5. Conclusion

In this paper, a BG model which predicts the energy harvesting with piezoelectric cantilever beam on a vehicle suspension has been presented. It is distinguished from existing modeling work on energy harvesting system in that it is amenable to estimate the energy harvested through a realistic and complete system, i.e. composed of the car suspension, the energy beam harvester and the restitution circuit while capturing all the multi-physic domains and power exchange between all the subsystems.

In a first, the simulated frequency responses of the energy piezoelectric harvesting subsystem have been discussed and verified by comparing them with experimental results performed in a laboratory environment in order to meet the Technology Readiness Level 5 index. In a second step, road tests have been successfully performed and compared with simulation results. In addition, a simulation of the complete system has been proposed with an analysis allowing extracting injected, stored and dissipated powers in both mechanical and electrical domains and for all subsystems as function of time and for the case of a speed bump solicitation. In view of an energy balance, small

power but with a long duration harvesting is obtained. Therefore, energy harvester may be interesting for a punctual use with a large period of electrical loading

In summary, the built model enables us thus to predict and perform an analysis of the power harvesting efficiency through a complete and realistic system. It is our aim that the model presented in this paper may be used and developed further for the use and design of other energy harvesting systems or for others kinds of applications.

Future work will be focused on two aspects. First, a low-frequency demonstrator will be built on a real suspension system proposed by the society SOBEN and tested on a car driven on a road. The second direction of future work is the application of the modeling approach for the use of an electromagnetic harvester. There is also a large interest to harvest high displacement energy generated in such a suspension system and this harvesting technique could also complete the preceding ones.

References

[1] Vullers RJM, Van Schaijk R, Visser HJ, Penders J, Van Hoof C. Autonomous wireless sensor networks. IEEE Solid-state Circuits Mag 2010;2(2):29–38.
[2] Delebarre C, Grondel S, Rivart F. Autonomous piezoelectric structural health monitoring system for on-production line use. Adv Appl Ceram Struct Funct Bioceramics 2015;14(4).
[3] Triplett CG, Christi C. 'Vehicular mounted piezoelectric generator',US7429805, 1985.
[4] Snyder DS. 'Piezoelectric reed power supply for use in abnormal tire condition warning systems', US4504761, 1985.
[5] Khameneifar F, Arzanpour S. Energy harvesting from pneumatic tires using piezoelectric transducers. ASME conference on smart materials, adaptive structures and intelligent systems, smasis08. Turf Valley Resort, Ellicott City, Maryland, USA October; 2008. p. 28–30.
[6] van den Ende DA, van de Wiel HJ, Groen WA, van der Zwaag S. Direct strain energy harvesting in automobile tires using PZT-polymer composites. Smart Mater Struct 2012;21:1–11.
[7] Lee J, Choi B. Development of a piezoelectric energy harvesting system for implementing wireless sensors on the tires. Energy Convers Manage 2014;78:32–8.
[8] Wu L, Wang Y, Jia C, Zhang C. Battery-less piezoceramics mode energy harvesting for automobile TPMS. 8th International conference on ASIC, ASICON'09. 2009. p. 1205–8.
[9] Singh KB, Bedekar V, Taheri S, Priya S. Piezoelectric vibration energy harvesting system with an adaptive frequency tuning mechanism for intelligent tires. Mechatronics 2012;22:970–88.
[10] Balasubramaniam M, Fortin JB, Smith WJ, Luo H. 'Energy harvesting system, apparatus and method', US7116036, 2006.
[11] Olivier JR, Neurgaonkar RR, Moffatt AP, Khoshnevisan M, Nelson JG. 'Piezoelectric energy harvester and method', US6407484, 2002.
[12] Roundy S. Energy harvesting for tire pressure monitoring systems: design considerations. Proceedings of PowerMEMS 2008 + microEMS 2008. 2008. pp. 1-6, Sendai, Japan, November 9-12.
[13] Renuke PA. Dynamic analysis of a car chassis. Int J Eng Res Appl 2012;2(6):955–9.
[14] Verros G, Natsiavas S, Papadimitriou C. Design optimization of quarter-car models with passive and semi-active suspensions under random road excitation. J Vib Control 2005;11(5):581–606.
[15] Tamboli JA, Joshi SG. Optimum design of a passive suspension system of a vehicle subjected to actual random road excitations. J Sound Vib 1999;219(2):193–205.
[16] Rustighi E, Elliott SJ, Finnveden S, Gulyás K, Mócsai T, Danti M. Linear stochastic evaluation of tyre vibration due to tyre/road excitation. J Sound Vib 2008;310(4):1112–27.
[17] Jha SK. Characteristics and sources of noise and vibration and their control in motor cars. J Sound Vib 1976;47(4):543–58.
[18] Gonçalves JP, Ambrósio JA. Optimization of vehicle suspension systems for improved comfort of road vehicles using flexible multibody dynamics. Nonlinear Dyn 2003;34(1):113–31.
[19] Li H, Tian C, Deng ZD. Energy harvesting from low frequency applications using piezoelectric materials. Appl Phys Rev 2014;1(4):1–20.
[20] Erturk A, Inman DJ. A distributed parameter electromechanical model for cantilevered piezoelectric energy harvesters. J Vib Acoust 2008;130:1–15.
[21] Erturk A, Inman D. An experimentally validated bimorph cantilever model for piezoelectric energy harvesting from cantilevered beams. Smart Mater Struct 2009;18:1–18.
[22] Erturk A. Assumed-modes modeling of piezoelectric energy harvesters: Euler–Bernouilli, Rayleigh, and Timoshenko models with axial deformation. Comput Struct 2012;106 – 107:214–27.
[23] Roundy S. On the effectiveness of vibration-based energy harvesting. J Intell Mater Syst Struct 2005;16:809–23.
[24] Love J. Process automation handbook – A guide to theory and practice. London: Springer; 2007.
[25] Busch-Vishniac IJ, Paynter HM. Bond Graph models of acoustical transducers. J Franklin Inst 1991;328(5-6):663–73.
[26] Sainthuile T, Grondel S, Delebarre C, Godts S, Paget C. Energy harvesting process modeling of an aeronautical structural health monitoring system using a Bond Graph approach. Int J Aerosp Sci 2012;1(5):107–15.
[27] Sainthuile T, Delebarre C, Grondel S, Paget C. Bond Graph model of a thin SHM piezoelectric energy harvester. 8th International workshop on structural health monitoring. 2011. Sept.
[28] Cauffriez L, Grondel S, Loslever P, Aubrun C. Bond Graph modeling for fault detection and isolation of a train door mechatronic system. Control Eng Pract 2016;49:212–24.
[29] Vahdati N, Heidari S. A novel semi-active fluid mount using a multi-layer piezoelectric beam. J Vib Control 2010.
[30] Goldfarb M, Celanovic N. A lumped parameter electromechanical model for describing the nonlinear behavior of piezoelectric actuators. J Dyn Syst Meas Control 1997;119(3):478–85.
[31] Margolis D, Shim T. A Bond Graph model incorporation sensors, actuators and vehicles dynamics. J Franklin Inst 2001;338(1):21–34.
[32] Filippini G, Nigro N, Junco S. 'Vehicle dynamics simulation using bond graph', Processing 3rd international conference IMAACA'2007, February, 2007.
[33] Silva LI, Magallan GA, De Angelo CH, Garcia GO. Vehicle dynamics using multi-bond graph: four wheel electric vehicle modeling. 34th Annual conference of IEEE industrial electronics, IECON 2008. 2008. p. 2846–51. 10-13 November.
[34] Silva LI, Magallan GA, de la Barrera PM, De Angelo CH, Gracia GO. Modeling of electric vehicles dynamics with multi-bond graphs. IEEE vehicle power and propulsion conference, VPPC, Lille. 2010. p. 1–3. September.
[35] Garcia-Tenorio C, Quijano N, Mojica-Nava E, Sofrony J. Bond Graph model-based for IDA-PBC. IEEE conference on control applications (CCA). 2016. p. 19–22. September.
[36] Khemliche M, Dif I, Latreche S, Bouamama BO. Modelling and analysis of an active suspension ¼ of vehicle with bond graph. First international symposium on control, communications and signal processing. Hammamet, Tunisia, Tunisia; 2004. p. 21–4. March.
[37] Nishida G, Takagi K, Maschke B, Osada T. Multi-scale distributed parameter modeling of ionic polymer-metal composite soft actuator. Control Eng Pract 2011;19(4):321–34.
[38] Bentefrit M, Grondel S, Soyer C, Fannir A, Cattan E, Madden JD, Nguyen TMG, Plesse C, Vidal F. Linear finite-difference bond graph model of an ionic polymer actuator. Smart Mater Struct 2017;26(9).
[39] Karnopp D. State variables and pseudo bond graphs for compressible thermofluid systems. J Dyn Syst Meas Control 1979;101(3):201–4.
[40] Wang G-Q, Lu Y-M. An improved lumped parameter model for a piezoelectric energy harvester in transverse vibration. Hindawi Publishing Corporation, Shock and Vibration; 2014. p. 1–12. 2014.
[41] Gillespie TD, Sayers MW, Segel L. Calibration of response-type road roughness measuring systems NCHRP; 1980. report, no. 228.
[42] Jazar RN. Vehicle dynamics: theory and application. US: Springer; 2008.
[43] Li B, Laviage AJ, You JH, Kim Y-J. Harvesting low-frequency acoustic energy using multiple PVDF beam arrays in quarter-wavelength acoustic resonator. Appl Acoust 2013;74:1271–8.
[44] Bert CW, Birman V. Effects of stress and electric field on the coefficients of piezoelectric materials: one-dimensional formulation. Mech Res Commun 1998;25(2):165–9.
[45] Erturk A, Inman DJ. Appendix c: modal analysis of a uniform cantilever with a tip mass. Piezoelectric Energy Harvesting 2011:353–66.
[46] Kong N, Sanha D, Erturk A, Inman D. Resistive impedance matching circuit for piezoelectric energy harvesting. J Intell Mater Syst Struct 2010;21:1293–302.
[47] Linear Technologie, 'LTC3588-1 Nanopower energy harvesting power supply', Available: http://cds.linear.com/docs/en/datasheet/35881fc.pdf.
[48] International Organization for Standardization. Mechanical vibration road surface profiles reporting of measured data Norme ISO 8608:1995Available https://www.iso.org/standard/15913.html; 1995.
[49] Aubouet S. 'Semi-active SOBEN suspensions modeling and control', 2010.
[50] Loprencipe G, Zoccali P. Use of generated artificial road profiles in road roughness evaluation. J Modern Transp 2017;25(1):24–33.